Multiscale Ommatidial Arrays with Broadband and Omnidirectional Antireflection and Antifogging Properties by Sacrificial Layer Mediated Nanoimprinting

Hemant Kumar Raut,[*,†,‡,□] Saman Safari Dinachali,[‡,□] Yee Chong Loke,[‡] Ramakrishnan Ganesan,[∥] Kwadwo Konadu Ansah-Antwi,[‡,⊥] Aleksander Góra,[†,§] Eng Huat Khoo,[#] V. Anand Ganesh,[□] Mohammad S. M. Saifullah,[*,‡] and Seeram Ramakrishna[†,§]

[†]Department of Mechanical Engineering, National University of Singapore, Singapore 117574, Republic of Singapore, [‡]Institute of Materials Research and Engineering, A*STAR (Agency for Science, Technology and Research), 3 Research Link, Singapore 117602, Republic of Singapore, [§]Centre for Nanofibers and Nanotechnology, National University of Singapore, Nanoscience and Nanotechnology Initiative, 2 Engineering Drive 3, Singapore 117576, Republic of Singapore, [∥]Department of Chemistry, Birla Institute of Technology & Science, Pilani—Hyderabad Campus, Jawahar Nagar, Shameerpet Mandal, Hyderabad 500 078, Telangana, India, [⊥]Department of Electrical and Computer Engineering, National University of Singapore, Singapore 117574, Republic of Singapore, [#]Electronics and Photonics Department, Institute of High Performance Computing, A*STAR (Agency for Science, Technology and Research), 1 Fusionopolis Way, Connexis, Singapore 138632, Republic of Singapore, and [□]Division of Engineering Product Development, Singapore University of Technology and Design, 8 Somapah Road, Singapore 487372, Republic of Singapore

ABSTRACT Moth's eye inspired multiscale ommatidial arrays offer multifunctional properties of great significance in optoelectronic devices. However, a major challenge remains in fabricating these arrays on large-area substrates using a simple and scalable technique. Here we present the fabrication of these multiscale ommatidial arrays over large areas by a distinct approach called sacrificial layer mediated nanoimprinting, which involves nanoimprinting aided by a sacrificial layer. The fabricated arrays exhibited excellent pattern uniformity over the entire patterned area. Optimum dimensions of the multiscale ommatidial arrays determined by the finite-difference time domain simulations served as the design parameters for replicating the arrays on glass. A broadband suppression of reflectance to a minimum of ~1.4% and omnidirectional antireflection for highly oblique angles of incidence up to 70° were achieved. In addition, superhydrophobicity and superior antifogging characteristics enabled the retention of optical properties even in wet and humid conditions, suggesting reliable optical performance in practical outdoor conditions. We anticipate that these properties could potentially enhance the performance of optoelectronic devices and minimize the influence of in-service conditions. Additionally, as our technique is solely nanoimprinting-based, it may enable scalable and high-throughput fabrication of multiscale ommatidial arrays.

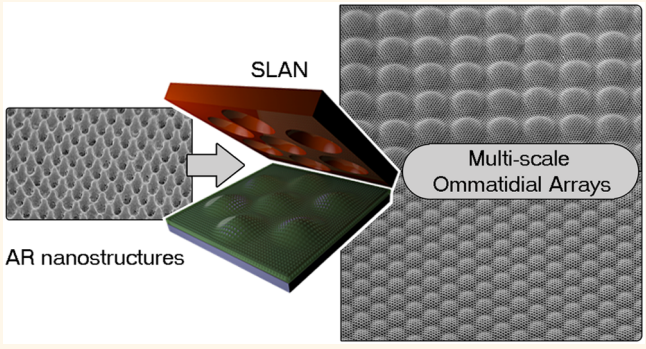

KEYWORDS: moth's eye antireflection · nanoimprint lithography · hierarchical patterning · superhydrophobicity · biomimetics

Eyes have been long-standing inspiration for the design of artificial visual systems.[1,2] In recent years profound design inspirations have come from compound eyes found in moths, butterflies, and other insects, which are remarkable for their advantages such as greater depth of field, wide-angle field of view, sensitivity to motion, and negligible aberration.[3−7] Compound eyes of moths, for instance, are a curvilinear design of hexagonally packed microlenses called ommatidia, which focus light onto the internal photoreceptors.[5] The surface of each ommatidium is further textured into patterns of hexagonally packed, subwavelength antireflective (AR)

* Address correspondence to hemant_raut@sutd.edu.sg, saifullahm@imre.a-star.edu.sg.

Received for review September 11, 2014 and accepted January 29, 2015.

Published online January 29, 2015
10.1021/nn5051272

nanostructures that produce a gradual transition in refractive index at the interface.[8,9] This helps in severe reduction in reflection of light, thereby enhancing the light sensitivity of the eyes of moths.[9,10] The AR nanostructures together with ommatidial arrays form an elegant framework of multiscale patterns that equip the nocturnal moths with an unsurpassed capability to see even in dim starlight.[11] The hierarchical patterns also enable their eyes to maintain unhindered vision in humid environments by resisting adherence of nucleated fog or raindrops on the eyes that could otherwise cause scattering of light.[12]

Microlens arrays, reminiscent of ommatidial architecture, are commonly used in many optoelectronic devices such as image sensors, biomimetic artificial eyes, light-emitting diodes, and solar energy devices to concentrate light on the photoactive region for fill-factor enhancements.[13−16] However, a portion of light incident on the lenses also gets reflected due to an abrupt change in refractive index at the interface. Reflection losses result in poor contrast reproduction in image sensors and reduced efficiency in solar energy devices.[17,18] Moreover, in image sensors, parts of reflected light propagating through adjacent microlenses can also result in crosstalk and poor signal-to-noise ratio, which can deteriorate image quality.[19] On the other hand, research on AR nanostructures on planar glass, silicon, and various other planar substrates has shown satisfactory reduction in reflection losses.[18,20,21] Following these cues, fabrication of multiscale ommatidial arrays has also received great attention in recent times, not just for minimizing reflection losses but also for obtaining multifunctional properties such as water repellency and antifogging.[6,7,12−15] Foremost approaches to fabricate these multiscale patterns involved the use of a moth's compound eye as a biological template.[22,23] Unfortunately, this approach is severely restricted by the small area and fixed diameter of the original ommatidia. Alternative approaches to fabricate the desired patterns combined multiple fabrication techniques and involved several steps such as fabrication of microlens arrays followed by self-assembly of nanospheres on the arrays and in some cases a final plasma etching through the nanosphere mask.[12,24−26] The presence of local defects and small pattern area also posed challenges to achieving uniform antireflection and antifogging properties and replicating these complex arrays on an industrial scale.[12]

In this paper, we report a sacrificial layer mediated nanoimprinting (SLAN) technique for the fabrication of multiscale ommatidial arrays on large-area substrates, which enabled us to incorporate antireflection, superhydrophobicity, and antifogging characteristics into the substrate. Nanoimprinting or nanoimprint lithography (NIL) is a simple pattern transfer technique, widely used to fabricate nanostructure patterns on various planar substrates.[27−30] It basically involves transfer of surface reliefs from a template to a thin film by embossing at an optimum combination of temperature and pressure. Furthermore, NIL offers a very good resolution with relatively faster replication and has proven to be economical.[27] However, for an effective pattern transfer onto a surface by the NIL technique, surface flatness is essential. A surface with microlens arrays naturally presents a challenge to applying NIL for further texturing to form hierarchical patterns. A recent report on fabrication of multiscale ommatidial arrays by point-by-point laser swelling of imprinted nanostructure patterns suffers from being time-consuming and also poses limitations in generating arbitrary microlens dimensions.[31] To overcome these challenges, our SLAN technique follows a distinctive approach of first fabricating the moth's eye AR nanostructure patterns on a thermoplastic film followed by imprinting of the microlens arrays. During the imprinting of the microlens arrays, a sacrificial layer encapsulates the nanostructure patterns and prevents any deformation of the nanostructures. Being fully NIL-based, the SLAN approach capitalizes on the scalability and high throughput of NIL and, thus, enables fabrication of multiscale ommatidial arrays on arbitrarily large-area substrates with a high degree of pattern uniformity and structural integrity. Replication of these arrays on glass substrates exhibits effective antireflection not only over a broad spectrum but also at increasingly oblique angles of incidence. The unique, multiscale texture also equipped the surface with superior fog resistance and superhydrophobic characteristics. These multifunctional properties enable the arrays to retain their superior optical properties in real-time environmental conditions.

RESULTS AND DISCUSSION

Fabrication of Multiscale Ommatidial Arrays. Figure 1 illustrates the SLAN process to fabricate the multiscale ommatidial arrays. In a first step, the moth's eye AR nanostructures were fabricated by imprinting the respective mold on a polycarbonate film (PC). The diameter and height of the nanostructures were ∼200 nm, and they were arranged in a hexagonal close packed (hcp) pattern in accordance with the AR nanostructures found in a biological moth. An SEM image of this planar moth's eye nanostructure array is shown alongside the illustration in Figure 1a. The imprinted surface was then spin-coated with a 20 wt % solution of poly(sodium 4-styrenesulfonate) (PSS) to form a thin film of ∼500 nm (Figure 1b). A second imprinting of the microlens arrays was then performed on the nanostructured patterns encapsulated in the PSS thin film, at a temperature higher than the glass transition temperature of PC. While the second imprinting was underway and the nanostructured surface was being molded into microlens arrays, the in-between PSS layer

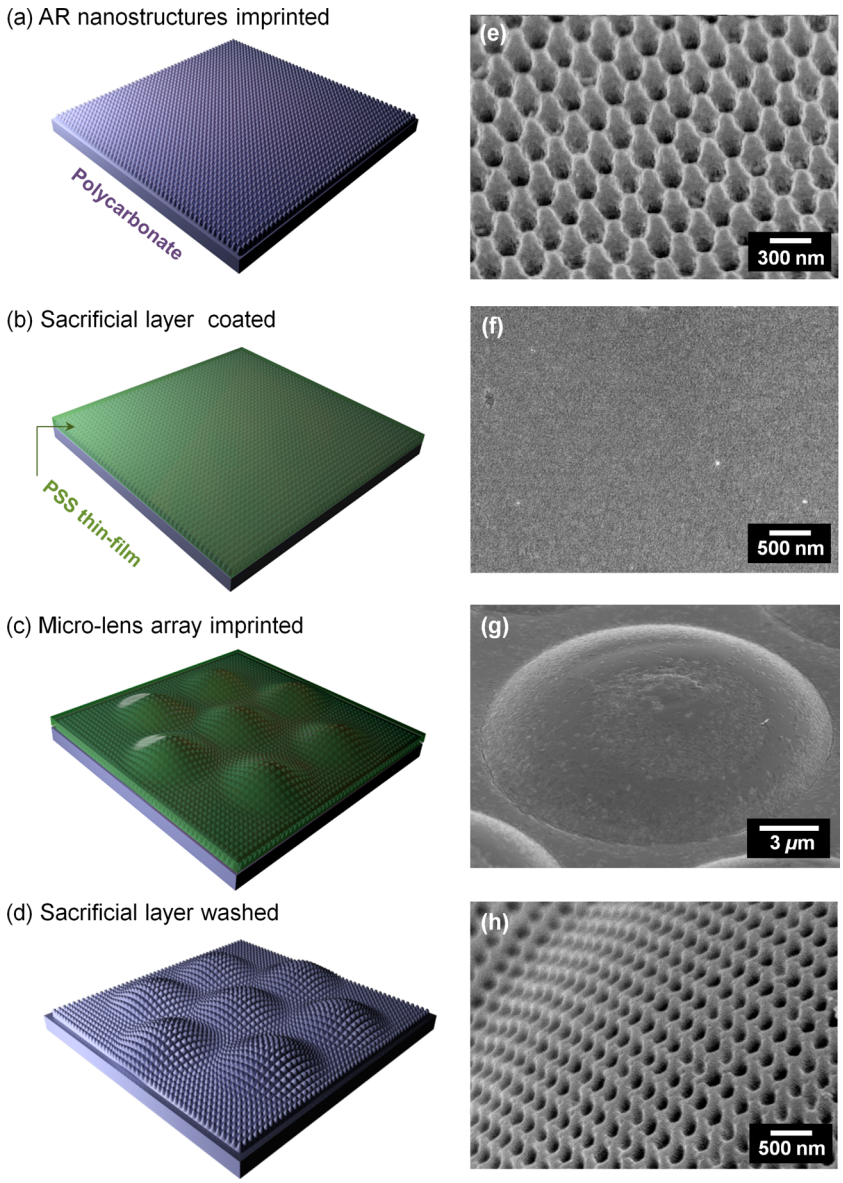

Figure 1. Fabrication of multiscale opmmatidial arrays by SLAN. Process steps shown in the schematic are as follows: (a) Imprinting of moth's eye AR nanostructures on a flexible polycarbonate substrate. An SEM image on the right shows the actual nanostructure arrays. (b) Coating of a sacrificial layer of poly(sodium 4-styrenesulfonate), PSS, fully covering the nanostructure arrays as shown in the corresponding SEM image. (c) Imprinting microlens arrays over the moth's eye nanostructure arrays encapsulated within the sacrificial layer. SEM image on right shows a microlens after imprinting. The underlying AR nanostructures are hidden beneath the sacrificial layer. (d) Simple washing of the imprinted substrate in water, thereby removing the sacrificial layer. The SEM image on the right shows a curved section of the multiscale ommatidial arrays.

protected the underlying AR nanostructures from buckling or deforming. An SEM image after this intermediate step, as displayed in Figure 1c, shows the PSS film covering the underneath multiscale structures. Since PSS has a melting temperature (T_m) of 450 °C, which is much higher than that of the PC (T_m = 155 °C), the former does not transform into a molten state and is able to firmly secure the AR nanostructures. After mold release, the imprinted substrate was immersed in water, leading to complete dissolution of PSS off the imprinted surface. Notably, this technique takes advantage of the preferential solubility of PSS and polycarbonate in polar and nonpolar solvents, respectively. Thus, highly uniform multiscale ommatidial arrays composing microlenses covered with AR nanostructure patterns on top were produced as shown in Figure 1d. The arrays were fully conformal to the curved portions of the ommatidia as well as flat interommatidial regions. As shown in Figure 1d, the AR nanostructures atop the microlenses preserved their protuberances after the completion of SLAN (further confirmed by the cross-sectional SEM image in the Supporting Information, Figure S2b). On the other hand, imprinting performed in the absence of the sacrificial layer, though carried out at relatively lower temperature, left the AR nanostructures severely deformed (Supporting Information,

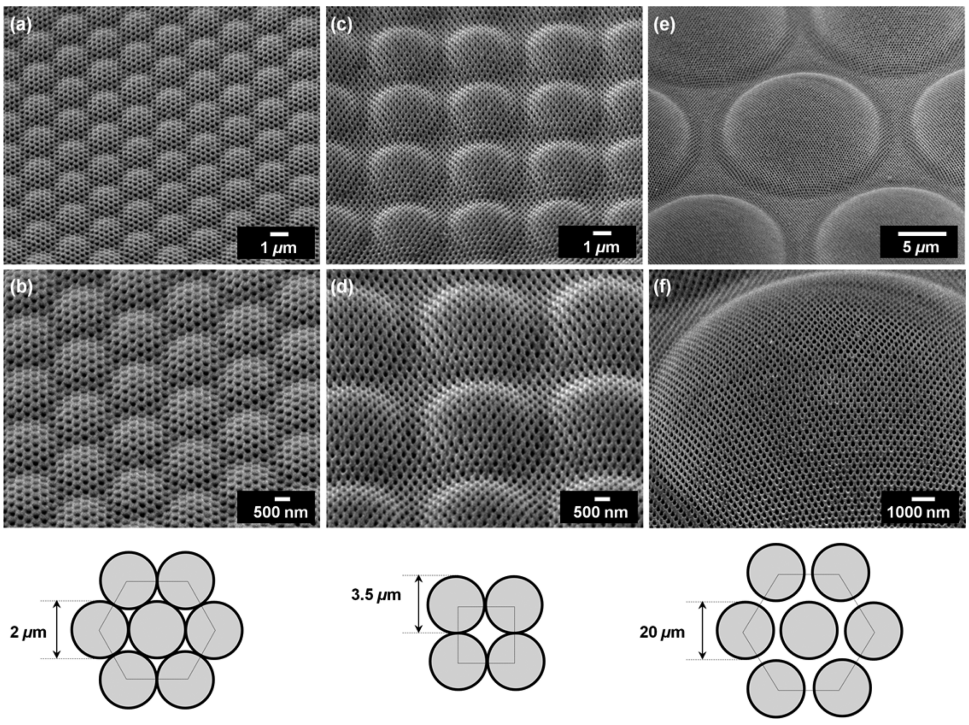

Figure 2. SEM images of the multiscale ommatidial arrays. Multiscale arrays in (a) and (e) show a hexagonal close-packed arrangement of individual microlenses, while (c) shows a square-packed configuration. Magnified SEM images of each variety of multiscale ommatidial array are shown in (b), (d), and (f) with details of ommatidial diameter in the bottom frame.

Figure S1a). In addition, a conventional approach involving sequential imprinting of AR nanostructures upon an array of microlenses did not fully replicate the nanostructures on the entire surface of the lenses (Supporting Information, Figure S1b).[32] We surmise that the curvature of the microlens prohibited conformal contact with the AR nanostructure mold during imprinting. On the other hand, the SLAN technique, being a fully NIL-reliant approach, facilitated the fabrication of the multiscale ommatidial arrays at a much faster speed over a larger area. Patterns were transferred with higher fidelity over the entire area of the substrate, indicating the potential for large-area manufacturing. Any minor defects present in the final multiscale ommatidial arrays were induced by surface defects present in the microlens molds, which were fabricated by a photoresist reflow technique.

Most compound eye-inspired optoelectronic devices currently use microlens arrays with diameters ranging from 25 to 2 μm.[33−35] In accordance with these prevailing size domains, we successfully fabricated a variety of multiscale ommatidial arrays of diameters from 2 to 20 μm with hexagonal and square-packed arrangements, as shown in Figure 2. Since the insect's compound eyes have ommatidia arranged in a hexagonal packing, we selected the 2 and 20 μm hexagonally packed multiscale ommatidial arrays for analysis of multifunctional properties. AFM images of these multiscale ommatidial arrays (Figure 3) provided the height and diameter of the ommatidia that formed the basis for modeling of the arrays for simulation studies as discussed in the next section. After fabricating the multiscale ommatidial arrays on a flexible substrate (Figure 4a), a secondary Ni mold comprising the pattern was prepared. This allowed us to directly imprint the multiscale ommatidial arrays on glass through a single-step imprinting, thereby further improving the process throughput. In order to replicate multiscale ommatidial arrays with robustness and durability, we used a previously reported hybrid polymer resin containing methacryl POSS for their fabrication on glass as shown in Figure 4b.[20]

Broadband and Omnidirectional AR Property of Multiscale Ommatidial Arrays. Multiscale ommatidial arrays can potentially enhance the light sensitivity of imaging devices and eliminate image glare by reducing reflection losses.[21,36−39] Reflectance reduction is also of significance in enhancing the efficiency of solar cells that use microlens arrays as light concentrators.[13] In order to determine the optimum diameter of the multiscale ommatidial arrays, we performed FDTD simulations with diameters of 2 and 20 μm while maintaining the same ommatidial contact angle and hexagonally packed configuration. By comparing the simulated reflectance, it was found that the multiscale ommatidial arrays with ommatidial diameter 20 μm showed the lowest reflectance (Supporting Information, Figure S3). We measured the hemispherical (specular + diffused) reflectance of the multiscale ommatidial arrays of ommatidial diameter 20 μm replicated on glass. The hemispherical reflectance of the multiscale ommatidial arrays, as shown in Figure 4c, displayed a

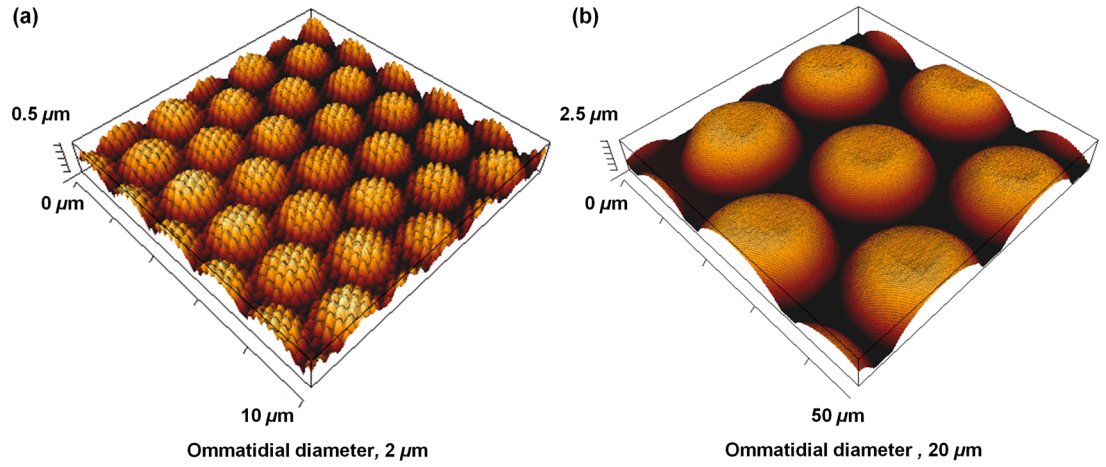

Figure 3. AFM images of the multiscale ommatidial arrays. Multiscale arrays of ommatidial diameter 2 and 20 μm are shown in (a) and (b) respectively.

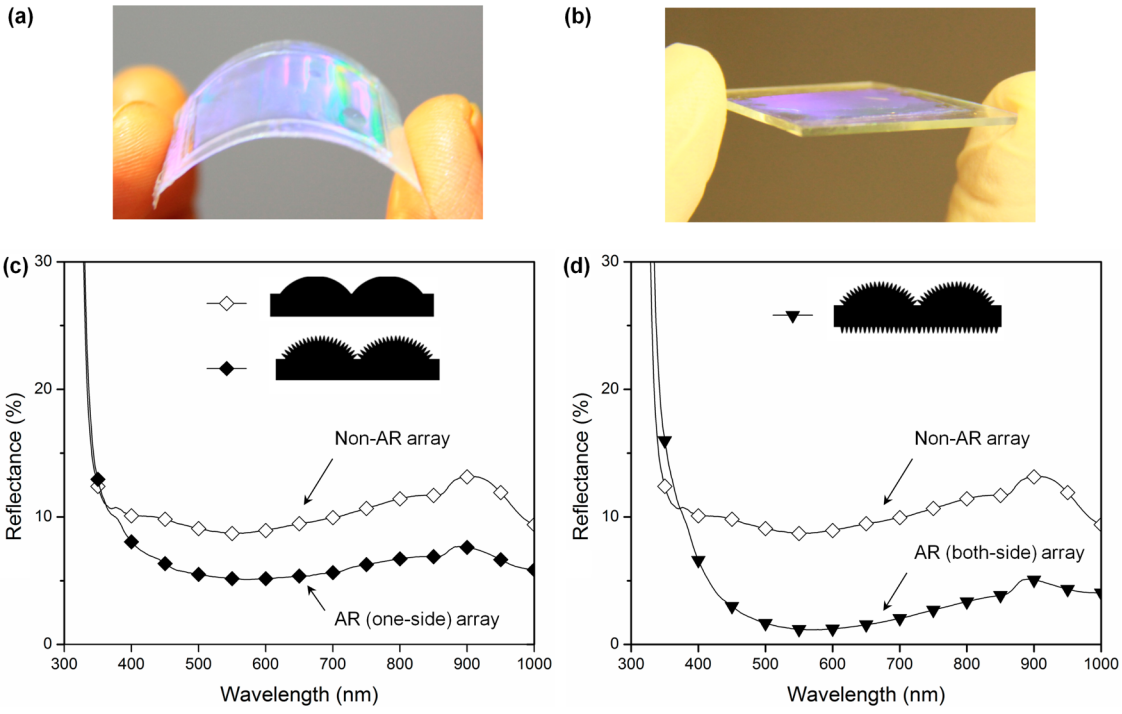

Figure 4. Optical properties of multiscale ommatidial arrays. (a) Large-area multiscale ommatidial arrays on a flexible PC film fabricated by the SLAN technique. (b) Multiscale ommatidial arrays comprising methacryl POSS, after replication on glass. Hemispherical reflectance curves of (c) multiscale ommatidial arrays with AR nanostructures only on the ommatidial side *versus* the non-AR ommatidial arrays and (d) multiscale ommatidial arrays with AR nanostructures present on both sides of the substrate. A broadband reduction in reflection could be seen in the plots. (Ommatidial diameter = 2 μm.)

broadband reduction in reflectance for wavelengths between 400 and 1000 nm, in comparison to the non-AR counterpart. A minimum reflection of ~8.7% of a non-AR ommatidial array was reduced to ~4.8% in the multiscale ommatidial array due to the presence of AR nanostructures. Formative studies on AR nanostructures in the compound eyes of moths have also shown an average of 4 percentage points reduction in reflectance off the ommatidial surface.[33,40] Since the multiscale ommatidial arrays were fabricated on a glass with a flat rear side, Fresnel reflections arising from the rear surface contributed to the overall reflectance. Covering the rear surface with moth's eye AR nanostructures further reduced the reflectance. A broadband reduction (400−1000 nm) in reflectance, with a minimum reflectance of 1.4% was observed in the multiscale ommatidial arrays equipped with AR nanostructures on both sides (Figure 4d). The reduction in reflectance is attributed to an axial gradient in refractive index at the interface, realized due to the unique shape of AR nanostructure patterns covering the microlenses as opposed to an abrupt change in index in microlenses without the AR nanostructures.[40,41] The minimum height (*h*) of the AR nanostructures can be theoretically

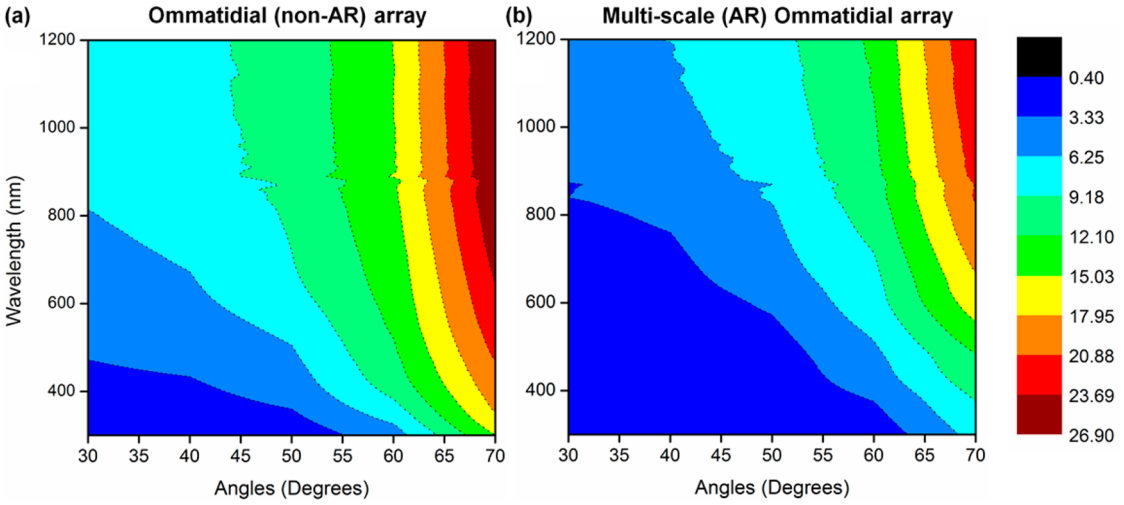

Figure 5. Omnidirectional antireflection of multiscale ommatidial arrays. Contour plots of reflectance *versus* wavelength measured over angles of incidence from 30° to 70° for (a) ommatidial arrays without AR nanostructures and (b) multiscale ommatidial arrays containing AR nanostructures on both sides. The rightmost panel shows the color depicting each band of reflectance.

determined by applying the condition for suppression of nonzero diffraction orders in the diffraction grating equation. It has been shown that for broadband antireflection $h < (\lambda/2)$.[42] This also implies that for AR nanostructures of height ~200 nm reflectance will gradually increase for wavelengths $\lambda < 400$ nm, which can be seen in the reflectance profiles of the multiscale ommatidial arrays in Figure 4.

Omnidirectional property is also an important characteristic of antireflective coatings because in solar cells, for instance, relatively higher reflection of light incident at increasingly oblique angles could affect the efficiency of the cell. Reflectance of the multiscale ommatidial arrays was measured as a function of the incident angles of light, between 0° and 70°, and a comparison with that of the non-AR ommatidial arrays is shown in Figure 5a and b. For angles of incidence up to 45°, the reflectance of the multiscale ommatidial arrays remained below 6% (within the blue regime of the contour plots shown in Figure 5b), almost over the entire spectral range of 300−1200 nm, while reflectance of the non-AR ommatidial arrays attained ~9% within the same spectral range. At relatively higher incident angles, between 40° and 60°, the reflectance of the non-AR ommatidial arrays reached ~15%, while the reflectance of the multiscale ommatidial arrays was between 3% and 9%. In fact, even at sharply oblique angles of incidence, ranging between 60° and 70°, relatively higher reflectance could be seen for the non-AR ommatidial array in Figure 5a (larger portion in red and brown regimes). The average reflectance of the multiscale ommatidial arrays was nearly six percentage points lower than that of the non-AR counterpart at these highly oblique angles of incidence.

Superhydrophobic Antifogging Property of Multiscale Ommatidial Arrays. While the multiscale patterns in moth's eyes enhance photon collection, the very same structures also resist adherence of raindrops or nucleated fog on the eyes of the insect.[12] Attachment of water droplets on the eyes can cause scattering of light, compromising their vision. It has been shown that a regular hierarchical roughness realized through multiscale patterns offers antifogging characteristics of far greater superiority than conventional lotus-leaf-inspired superhydrophobic surfaces.[43]

Generally, superhydrophobicity conferred through surface roughness can be interpreted by the Cassie−Baxter model, which considers a water droplet to rest partly on microstructured textures and partly on entrapped air pockets between the microstructures.[44−47] Since the multiscale ommatidial arrays present a textured interface at both micro- and submicrometer length scales, we measured the contact angles formed by micrometric water droplets on their surface. Figure 6a shows the increase in water contact angle (WCA) as the surface texture became progressively multiscale, namely, from planar to hcp microlens arrays and finally to multiscale ommatidial arrays. Characteristic geometric length scales and feature morphologies also influence the degree of superhydrophobicity.[48,49] With an increase in ommatidial diameter from 2 μm to 20 μm, we observed a noticeable improvement in the WCA, as shown in Figure 6a. Finally, when we replicated the multiscale ommatidial arrays on glass using the methacryl POSS-containing resin, we obtained a WCA of ~151 $\pm$ 0.5°, as shown in Figure 6b. Additionally, apparent advancing (θ_a) and receding (θ_r) WCA for the multiscale ommatidial arrays were measured to be 152.0 $\pm$ 1° and 150.8 $\pm$ 1°, respectively, which indicates a low contact angle hysteresis: $(\theta_a - \theta_r) \leq 2°$. Experimentally, the contact angle hysteresis shows the inclination at which a droplet pinned on a surface becomes unstable under gravity and starts to roll off.[44] The enhanced water repellency of the multiscale

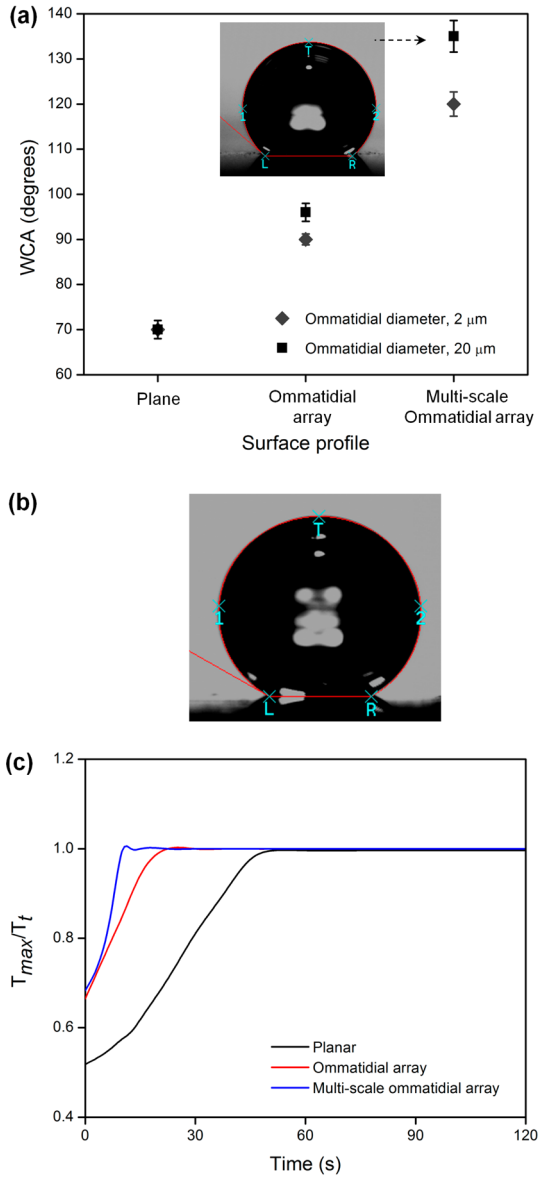

Figure 6. Superhydrophobicity and antifogging characteristics. (a) Water contact angle (WCA) on surfaces with progressively multiscale texturing. The multiscale ommatidial arrays show the highest increase in WCA. (b) WCA measured ~151° on multiscale ommatidial arrays, made of methacryl POSS, replicated on glass. (c) Antifogging property of multiscale ommatidial arrays quantified by performing time-lapse transmittance measurements (T_t) to determine time taken to regain original optical properties (T_{max}). Multiscale ommatidial arrays show significantly faster recovery from fogging.

ommatidial arrays fabricated on glass can be attributed to both the multiscale texture and the presence of the fluorinated monomer HDMA in the resist.

Fogging, on the other hand, presents a scenario where the intrinsic droplet dimensions, formed through condensation of water, are relatively small.[12] For a textured surface, an interstructural spacing larger than the dimensions of typical fog droplets and a relatively random arrangement of structures can cause pinning of the droplets. This seemingly causes wetting of a lotus leaf during fogging, which otherwise exhibits exceptional water repellency.[43] Since fogging results in a loss of transmittance, we quantified the response of the multiscale ommatidial arrays to fogging by measuring their transmittance at regular intervals (T_t) after exposure to a stream of saturated steam, until the original transmittance (T_{max}) was restored as described elsewhere.[32] As shown in Figure 6c, recovery from fogging was much faster in case of multiscale ommatidial arrays, as T_{max}/T_t reached a plateau in far less time than in the case of a planar surface. These properties of superhydrophobicity and antifogging are crucial in retaining the superior optical properties of the multiscale ommatidial arrays, especially in wet and humid environments.[12,18] Uniform packing density of the AR nanostructures in multiscale ommatidial arrays is crucial in obtaining the above properties, as any local defect could reduce the air fraction between the nanostructures.[12] Since the SLAN technique is capable of fabricating the multiscale ommatidial arrays with a high degree of uniformity over a large area, we observed a consistent WCA and antifogging property over the entire patterned area.

The precondition for an effective antireflection is an hcp arrangement of AR nanostructures. However, antifogging property is theoretically shown to improve by inculcating gaps between nanostructures as the hydrogen-bonded network of water molecules confronts a barrier to invade a critical separation of 100 nm.[50] Second, superhydrophobicity in most biological systems is an outcome of both hierarchical roughness and surface chemistry.[48,49] Thus, further improvements in superhydrophobicity and antifogging characteristics of the multiscale ommatidial arrays could be realized by incorporating these design specifications and exploring other resin formulations comprising fluorinated and siloxane moieties for their fabrication.

CONCLUSIONS

In conclusion, we have demonstrated a simpler fabrication of multiscale ommatidial arrays called sacrificial layer mediated nanoimprinting. The multiscale ommatidial arrays were fabricated by introducing a sacrificial layer atop a planar array of moth's eye nanostructures to protect them during molding into microlens arrays. This enables realization of multiscale ommatidial arrays over a large area with greater pattern fidelity. Finite-difference time domain (FDTD) simulations of these multiscale ommatidial arrays showed that structures of 20 μm diameter offered the lowest reflectance, which was verified experimentally. Additionally, these arrays exhibit multifunctional properties such as broadband and omnidirectional antireflection as well as superhydrophobic and antifogging characteristics, which are of potential application in image sensors, solar cells, LEDs, and numerous

other micro-optic components. Imprinting templates fabricated with the SLAN technique could also be employed in roll-to-roll and roll-to-plate nanoimprinting to reproduce the multiscale ommatidial arrays on flexible and flat substrates, respectively, with high volume.[51,52] It also presents a potential pathway for fabrication of various other biologically inspired multiscale patterns with immensely diverse applications.[53]

MATERIALS AND METHODS

Materials. Flexible polycarbonate sheets of 1 mm thickness were purchased from Goodfellow Cambridge Limited, UK. Poly(sodium 4-styrenesulfonate) solution (20 wt % in water) was purchased from Sigma-Aldrich. Ultrapure Millipore water was used in all the experiments. Methacryl POSS cage mixture (fw = 1433.97 g/mol) was purchased from Hybrid Plastics, Inc. It was used as-received. The initiator, benzoyl peroxide, was purchased from Lancaster Synthesis and was used without further purification. 1,6-Hexanediol diacrylate (Alfa Aesar) was used as a cross-linker. 3,3,4,4,5,5,6,6,7,7,8,8,9,9,10,10,10-Heptadecafluorodecyl methacrylate (HDMA) was purchased from Sigma-Aldrich.

Nanoimprint Lithography. A moth's eye nanostructure containing a Ni mold (3 cm × 2.5 cm) was used to imprint the AR nanostructures. Microlens molds of diameters 2 μm (hexagonally packed), 3.5 μm (square packed), and 20 μm (hexagonally packed) were fabricated by a photoresist reflow of pillar arrays discussed elsewhere and replicated into Ni molds.[54] For effective comparison of the properties of the final multiscale ommatidial arrays, the contact angles of the microlenses were kept nearly the same (Table ST1 in the Supporting Information). A Karl Süss mask aligner (MA6) was used to fabricate the pillar arrays of predetermined dimensions and center-to-center distance. All the molds were thoroughly cleaned by treating with oxygen plasma. A self-assembled monolayer (SAM) coating of 1*H*,1*H*,2*H*,2*H*-perfluorodecyltrichlorosilane was carried out on the Ni molds to decrease their surface energy and ensure easier demolding. An Obducat imprinter (Obducat, Sweden) was used to perform the imprinting. For replication of the multiscale patterns on glass, a resin containing a mixture of methacryl POSS and 1,6-hexanediol diacrylate was used as described elsewhere.[20] A 4 wt % of HDMA in the resist facilitated easier demolding by lowering the surface energy of the imprint.

Characterization of Multiscale Ommatidial Arrays. The hemispherical (specular and diffused) reflectance measurements for the samples were performed using a Shimadzu SolidSpec 3700 UV−vis−NIR spectrometer equipped with an integrating sphere attachment. Reflectance measurements at different angles of incidence were performed by using a variable-angle reflectance measurement accessory attached to the spectrometer. The morphology of the multiscale ommatidial arrays was studied by a JEOL JSM-6700F field-emission scanning electron microscope (FE-SEM) operating at 5 kV. Atomic force microscope (AFM) measurements were done using a NanoWizard3 (JPK, Germany) setup. Sharp cantilevers of resonance frequency of 300 kHz and force constant of 40 N/m (Budget Sensors Tap300-G, Bulgaria) were used. All cantilevers were used without previous treatment, and resonance frequency was set at 90% of maximum resonance frequency. Pictures of resolution 2048 × 2048 were obtained and analyzed with JPK Data Processing Software (version spm-4.3.39, JPK, Germany).

The water contact angle measurements were performed using a contact angle measurement setup (VCA Optima contact angle equipment from AST Products) in static sessile drop mode at room temperature. The contact angle values reported were averaged over at least five measurements performed over different areas of the sample. Fogging of the samples was performed by exposure to a stream of saturated steam as discussed elsewhere.[55] Transmittance measurements were repeated for the fogged samples using the Shimadzu SolidSpec 3700 UV−vis−NIR spectrometer over a bandwidth of 500−600 nm for 240 s.

FDTD Simulations. Simulations of reflectance for the multiscale ommatidial arrays were performed by commercially available FDTD Solutions 8.0 (Lumerical Solutions, Inc.).[20] Multiscale ommatidial arrays having an ommatidial diameter of 2 and 20 μm arranged in a hexagonal packing configuration were modeled, based on dimensions obtained from SEM and AFM measurements. The moth's eye nanostructures on the ommatidia were also modeled based on a hexagonal packing geometry with dimensions equal to those obtained from SEM observations. The dielectric constant for the multiscale ommatidial arrays was based on the (*n*, *k*) data obtained from the ellipsometric measurements of polycarbonate. The simulation used a nonuniform grid to model various parts of the ommatidial arrays. For the AR nanostructure patterns, the grid size was 5 nm in the *x*, *y*, and *z* directions. For the ommatidia of diameter 2 and 20 μm, the grid size was 20 and 200 nm, respectively. The use of nonuniform mesh allowed precise calculation and simulation at different parts of the multiscale ommatidial arrays with efficient usage of memory. Periodic boundary conditions were set for the *x* and *y* directions, and perfectly matched layer (PML) boundary conditions were set for the *z* direction. A plane-wave source was directed along the *z*-axis to calculate the reflectance of the multiscale ommatidial arrays. A monitor was set behind the plane-wave source to ensure correct measurement of the reflected waves. An additional monitor was added at 10 μm after the arrays to ensure that the total transmitted power was correct.

Conflict of Interest: The authors declare no competing financial interest.

Acknowledgment. The authors would like to acknowledge the help of Mr. Vincent Lim of the Institute of Materials Research and Engineering (IMRE) for help in preparation of the masks used in this work. H.K.R. would like to acknowledge the help of Dr. Marc Plaum and his team, from DSM Technologies Ltd., The Netherlands, for their help in measurements of reflectance at variable angles of incidence. Further, he would like to acknowledge the fellowship from the National University of Singapore for undertaking his Ph.D. studies.

Supporting Information Available: Three supplementary figures and one supplementary table. Figure S1 shows the deformed AR nanostructures due to imprinting performed in the absence of a sacrificial layer and incompletely imprinted AR nanostructures through an alternative sequential nanoimprinting approach for fabrication of the multiscale ommatidial arrays. Figure S2 shows the planar arrays of AR nanostructures, which after undergoing SLAN fabrication transform into multiscale ommatidial arrays. This is shown in the cross-sectional SEM images of the multiscale ommatidial arrays in Figure S2. Figure S3 shows the reflectance graphs obtained from the FDTD simulations of light incident on the multiscale ommatidial arrays of different diameters. Table ST1 shows the design parameters of the multiscale ommatidial arrays studied in this work. This material is available free of charge *via* the Internet at http://pubs.acs.org.

REFERENCES AND NOTES

1. Land, M. F.; Nilsson, D. E. *Animal Eyes*; Oxford University Press: Oxford, 2002.
2. Ko, H. C.; Stoykovich, M. P.; Song, J.; Malyarchuk, V.; Choi, W. M.; Yu, C. J.; Geddes, J. B.; Xiao, J.; Wang, S.; Huang, Y.; *et al.* A Hemispherical Electronic Eye Camera Based on Compressible Silicon Optoelectronics. *Nature* **2008**, *454*, 748–753.
3. Warrant, E.; Nilsson, D. E. *Invertebrate Vision*; Cambridge University Press: Cambridge, 2006.

4. Dudley, R. *The Biomechanics of Insect Flight: Form, Function, Evolution*; Princeton University Press: Princeton, NJ, 2000.
5. Exner, S.; Hardie, R. C. *The Physiology of the Compound Eyes of Insects and Crustaceans: A Study*; Springer-Verlag: Berlin, 1989.
6. Jeong, K. H.; Kim, J.; Lee, L. P. Biologically Inspired Artificial Compound Eyes. *Science* **2006**, *312*, 557–561.
7. Song, Y. M.; Xie, Y.; Malyarchuk, V.; Xiao, J.; Jung, I.; Choi, K. J.; Liu, Z.; Park, H.; Lu, C.; Kim, R. H.; *et al.* Digital Cameras with Designs Inspired by the Arthropod Eye. *Nature* **2013**, *497*, 95–99.
8. Bernhard, C. G.; Miller, W. H. A Corneal Nipple Pattern in Insect Compound Eyes. *Acta Physiol. Scand.* **1962**, *56*, 385–386.
9. Bernhard, C. G.; Miller, W. H.; Møller, A. R. The Insect Corneal Nipple Array. A Biological, Broad-band Impedance Transformer That Acts as an Antireflection Coating. *Acta Physiol. Scand.* **1965**, *63* (Suppl. 243), 1–79.
10. Wilson, S. J.; Hutley, M. C. The Optical Properties of 'Moth Eye' Antireflection Surfaces. *Opt. Acta: Int. J. Opt.* **1982**, *29*, 993–1009.
11. Kelber, A.; Balkenius, A.; Warrant, E. J. Scotopic Colour Vision in Nocturnal Hawkmoths. *Nature* **2002**, *419*, 922–925.
12. Gao, X.; Yan, X.; Yao, X.; Xu, L.; Zhang, K.; Zhang, J.; Yang, B.; Jiang, L. The Dry-Style Antifogging Properties of Mosquito Compound Eyes and Artificial Analogues Prepared by Soft Lithography. *Adv. Mater.* **2007**, *19*, 2213–2217.
13. MacMillan, H. F.; Hamaker, H. C.; Kaminar, N. R.; Kuryla, M. S.; Ristow, M. L.; Liu, D. D.; Virshup, G. F.; Gee, J. M. 28% Efficient GaAs Concentrator Solar Cells. *Conf. Rec. IEEE Photovoltaic Spec. Conf.* **1988**, *461*, 462–468.
14. Thomschke, M.; Reineke, S.; Lüssem, B.; Leo, K. Highly Efficient White Top-Emitting Organic Light-Emitting Diodes Comprising Laminated Microlens Films. *Nano Lett.* **2012**, *12*, 424–428.
15. Möller, S.; Forrest, S. R. Visual Improved Light Out-coupling in Organic Light Emitting Diodes Employing Ordered Microlens Arrays. *J. Appl. Phys.* **2002**, *91*, 3324–3327.
16. Watson, E. A.; Miller, D. T.; Barnard, K. J. Fill Factor Improvement Using Microlens Arrays. *Proc. SPIE* **1998**, *3276*, 123–134.
17. Hon-Sum, W. Technology and Device Scaling Considerations for CMOS Imagers. *IEEE Trans. Electron Devices* **1996**, *43*, 2131–2142.
18. Raut, H. K.; Ganesh, V. A.; Nair, A. S.; Ramakrishna, S. Anti-Reflective Coatings: A Critical, In-Depth Review. *Energy Environ. Sci.* **2011**, *4*, 3779–3804.
19. Agranov, G.; Berezin, V.; Tsai, R. H. Crosstalk and Microlens Study in a Color CMOS Image Sensor. *IEEE Trans. Electron Devices* **2003**, *50*, 4–11.
20. Raut, H. K.; Dinachali, S. S.; He, A. Y.; Ganesh, V. A.; Saifullah, M. S. M.; Law, J.; Ramakrishna, S. Robust and Durable Polyhedral Oligomeric Silsesquioxane-Based Anti-Reflective Nanostructures with Broadband Quasi-Omnidirectional Properties. *Energy Environ. Sci.* **2013**, *6*, 1929–1937.
21. Lee, C.; Bae, S. Y.; Mobasser, S.; Manohara, H. A Novel Silicon Nanotips Antireflection Surface for the Micro Sun Sensor. *Nano Lett.* **2005**, *5*, 2438–2442.
22. Ko, D. H.; Tumbleston, J. R.; Henderson, K. J.; Euliss, L. E.; DeSimone, J. M.; Lopez, R.; Samulski, E. T. Biomimetic Microlens Array with Antireflective "Moth-Eye" Surface. *Soft Matter* **2011**, *7*, 6404–6407.
23. Huang, J.; Wang, X.; Wang, Z. L. Bio-Inspired Fabrication of Antireflection Nanostructures by Replicating Fly Eyes. *Nanotechnology* **2008**, *19*, 025602.
24. Xu, H.; Lu, N.; Shi, G.; Qi, D.; Yang, B.; Li, H.; Xu, W.; Chi, L. Biomimetic Antireflective Hierarchical Arrays. *Langmuir* **2011**, *27*, 4963–4967.
25. Wu, F.; Shi, G.; Xu, H.; Liu, L.; Wang, Y.; Qi, D.; Lu, N. Fabrication of Antireflective Compound Eyes by Imprinting. *ACS Appl. Mater. Interfaces* **2013**, *5*, 12799–12803.
26. Yanagishita, T.; Nishio, K.; Masuda, H. Anti-Reflection Structures on Lenses by Nanoimprinting Using Ordered Anodic Porous Alumina. *Appl. Phys. Express* **2009**, *2*, 022001.
27. Costner, E. A.; Lin, M. W.; Jen, W. L.; Willson, C. G. Nanoimprint Lithography Materials Development for Semiconductor Device Fabrication. *Annu. Rev. Mater. Res.* **2009**, *39*, 155–180.
28. Dinachali, S. S.; Saifullah, M. S. M.; Ganesan, R.; Thian, E. S.; He, C. A Universal Scheme for Patterning of Oxides *via* Thermal Nanoimprint Lithography. *Adv. Funct. Mater.* **2013**, *23*, 2201–2211.
29. Dinachali, S. S.; Dumond, J.; Saifullah, M. S. M.; Ansah-Antwi, K. K.; Ganesan, R.; Thian, E. S.; He, C. Large Area, Facile Oxide Nanofabrication *via* Step-and-Flash Imprint Lithography of Metal-Organic Hybrid Resins. *ACS Appl. Mater. Interfaces* **2013**, *5*, 13113–13123.
30. Chou, S. Y.; Krauss, P. R.; Renstrom, P. J. Imprint Lithography with 25-Nanometer Resolution. *Science* **1996**, *272*, 85–87.
31. Shao, J.; Ding, Y.; Wang, W.; Mei, X.; Zhai, H.; Tian, H.; Li, X.; Liu, B. Generation of Fully-Covering Hierarchical Micro-/Nano-Structures by Nanoimprinting and Modified Laser Swelling. *Small* **2014**, *10*, 2595–2601.
32. Shi, G.; Lu, N.; Xu, H.; Wang, Y.; Shi, S.; Li, H.; Li, Y.; Chi, L. Fabrication of Hierarchical Structures by Unconventional Two-Step Imprinting. *J. Colloid Interface Sci.* **2012**, *368*, 655–659.
33. Stavenga, D. G.; Foletti, S.; Palasantzas, G.; Arikawa, K. Light on the Moth-Eye Corneal Nipple Array of Butterflies. *Proc. R. Soc. B* **2006**, *273*, 661–667.
34. Meyer-Rochow, V. B.; Stringer, I. A. N. A System of Regular Ridges Instead of Nipples on a Compound Eye That Has to Operate near the Diffraction Limit. *Vision Res.* **1993**, *33*, 2645–2647.
35. Huo, Y.; Fesenmaier, C. C.; Catrysse, P. B. Microlens Performance Limits in Sub-2μm Pixel CMOS Image Sensors. *Opt. Express* **2010**, *18*, 5861–5872.
36. Greiner, B. Adaptations for Nocturnal Vision in Insect Apposition Eyes. *Int. Rev. Cytol.* **2006**, *250*, 1–46.
37. Schuster, J.; Bellotti, E. Numerical Simulation of Crosstalk in Reduced Pitch HgCdTe Photon-Trapping Structure Pixel Arrays. *Opt. Express* **2013**, *21*, 14712–14727.
38. Raut, H. K.; Nair, A. S.; Dinachali, S. S.; Ganesh, V. A.; Walsh, T. M.; Ramakrishna, S. Porous SiO_2 Anti-Reflective Coatings on Large-Area Substrates by Electrospinning and Their Application to Solar Modules. *Sol. Energy Mater. Sol.* **2013**, *111*, 9–15.
39. Raut, H. K.; Dinachali, S. S.; Ansah-Antwi, K. K.; Ganesh, V. A.; Ramakrishna, S. Fabrication of Highly Uniform and Porous MgF_2 Anti-Reflective Coatings by Polymer-Based Sol−Gel Processing on Large-Area Glass Substrates. *Nanotechnology* **2013**, *24*, 505201.
40. Miller, W. H. Ocular optical filtering. In *Handbook of Sensory Physiology*; Autrum, H., Ed.; Springer-Verlag: Berlin, 1979; pp 69−143.
41. Rayleigh, L. On Reflection of Vibrations at the Confines of Two Media between Which the Transition is Gradual. *Proc. London Math. Soc.* **1879**, *s1*, 51–56.
42. Neviere, M.; Popov, E. *Light Propagation in Periodic Media: Differential Theory and Design*; Marcel Dekker: New York, 2002.
43. Cheng, Y. T.; Rodak, D. E. Is the Lotus Leaf Superhydrophobic? *Appl. Phys. Lett.* **2005**, *86*, 144101.
44. Cassie, A. B. D.; Baxter, S. Wettability of Porous Surfaces. *Trans. Faraday Soc.* **1944**, *40*, 546–551.
45. Ganesh, V. A.; Dinachali, S. S.; H. K; Walsh, T. M.; Nair, A. S.; Ramakrishna, S. Electrospun SiO_2 Nanofibers as a Template to Fabricate a Robust and Transparent Superamphiphobic Coating. *RSC Adv.* **2013**, *3*, 3819–3824.
46. Ganesh, V. A.; Nair, A. S.; Raut, H. K.; Walsh, T. M.; Ramakrishna, S. Photocatalytic Superhydrophilic TiO_2 Coating on Glass by Electrospinning. *RSC Adv.* **2012**, *2*, 2067–2072.
47. Ganesh, V. A.; Nair, A. S.; Raut, H. K.; Tan, T. T. Y.; He, C.; Ramakrishna, S.; Xu, J. Superhydrophobic Fluorinated POSS−PVDF-HFP Nanocomposite Coating on Glass by Electrospinning. *J. Mater. Chem.* **2012**, *22*, 18479–18485.

48. Kim, P.; Kreder, M. J.; Alvarenga, J.; Aizenberg, J. Hierarchical or Not? Effect of the Length Scale and Hierarchy of the Surface Roughness on Omniphobicity of Lubricant-Infused Substrates. *Nano Lett.* **2013**, *13*, 1793–1799.
49. Ganesh, V. A.; Raut, H. K.; Nair, A. S.; Ramakrishna, S. A Review on Self-Cleaning Coatings. *J. Mater. Chem.* **2011**, *21*, 16304–16322.
50. Lum, K.; Chandler, D.; Weeks, J. D. Hydrophobicity at Small and Large Length Scales. *J. Phys. Chem. B* **1999**, *103*, 4570–4577.
51. Ahn, S. H.; Guo, L. J. High-Speed Roll-to-Roll Nanoimprint Lithography on Flexible Plastic Substrates. *Adv. Mater.* **2008**, *20*, 2044–2049.
52. Ahn, S. H.; Guo, L. J. Large-Area Roll-to-Roll and Roll-to-Plate Nanoimprint Lithography: A Step toward High-Throughput Application of Continuous Nanoimprinting. *ACS Nano* **2009**, *3*, 2304–2310.
53. Bae, W. G.; Kim, H. N.; Kim, D.; Park, S. H.; Jeong, H. E.; Suh, K. Y. Scalable Multiscale Patterned Structures Inspired by Nature: The Role of Hierarchy. *Adv. Mater.* **2014**, *26*, 675–700.
54. Popovic, Z. D.; Sprague, R. A.; Neville-Connell, G. A. Technique for the Monolithic Fabrication of Microlens Arrays. *Appl. Opt.* **1988**, *27*, 1281–1284.
55. Park, K. C.; Choi, H. J.; Chang, C. H.; Cohen, R. E.; McKinley, G. H.; Barbastathis, G. Nanotextured Silica Surfaces with Robust Superhydrophobicity and Omnidirectional Broadband Supertransmissivity. *ACS Nano* **2012**, *6*, 3789–3799.